

Nanoscale

Accepted Manuscript



This is an *Accepted Manuscript*, which has been through the Royal Society of Chemistry peer review process and has been accepted for publication.

Accepted Manuscripts are published online shortly after acceptance, before technical editing, formatting and proof reading. Using this free service, authors can make their results available to the community, in citable form, before we publish the edited article. We will replace this *Accepted Manuscript* with the edited and formatted *Advance Article* as soon as it is available.

You can find more information about *Accepted Manuscripts* in the [Information for Authors](#).

Please note that technical editing may introduce minor changes to the text and/or graphics, which may alter content. The journal's standard [Terms & Conditions](#) and the [Ethical guidelines](#) still apply. In no event shall the Royal Society of Chemistry be held responsible for any errors or omissions in this *Accepted Manuscript* or any consequences arising from the use of any information it contains.



Journal Name

COMMUNICATION

Extremely Low Frequency Alternating Magnetic Field Triggered and MRI Traced Drug Delivery by Optimized Magnetic Zeolitic Imidazolate Framework-90 Nanoparticles

Received 00th January 20xx,
Accepted 00th January 20xx

DOI: 10.1039/x0xx00000x

Jie Fang,^a Yong Yang,^a Wen Xiao,^a Bingwen Zheng,^b Yun-Bo Lv,^a Xiao-Li Liu^a and Jun Ding*^a

www.rsc.org/

An extremely low frequency alternating magnetic field (ELF-AMF) is demonstrated to be able to effectively trigger the drug release from carefully engineered magnetic ZIF-90 nanoparticles. The embedded Fe₃O₄ nanoparticles or alternatively Gd₂O₃ nanoparticles serve as effective MRI tracer for potential visualization of drug delivery to ensure the accuracy.

The stimuli-responsive drug delivery systems (DDSs) are receiving rising attention owing to their capability of providing a higher concentration of drug in the specific target tissue on command with minimal systematic effects. These smart systems require sensor/actuator effectively response to internal variables (pH, GSH and *etc.*) or external stimuli (light, heat, magnetic or electric field). However, the design of such sensor/actuator responsive to internal variables is truly challenging since the composition of the biological environment is complex and the changes caused by a pathological process are mostly of scarce magnitude.¹ Magnetic field is an effective stimulus with deep penetration capacity. HF-AMF, 50-400kHz, was employed to promote local heating known as magnetic hyperthermia, so that the cancer cells can be killed directly by heat or treated by drugs released from heat responsive carriers.²⁻⁷ Radiofrequency field, 100 kHz-300 GHz, was also exploited to trigger the release of doxorubicin (DOX) from nanochain comprised of iron oxide nanoparticles and liposome.⁸

However, there has also been wide concern about the bio-safety of using high frequency fields on human bodies. Besides the hyperthermia effect threatening the healthy cells and tissues, it was reported that HF-AMF may also cause peripheral

nerve and/or cardiac stimulation to the patient.⁹ In 2011, the radio frequencies of electromagnetic fields were qualified by IARC and WHO as possibly increasing the risk of malignant brain tumor development.¹⁰ Indeed, electric fields induced in tissue are proportional to external electric or magnetic frequency, thus high frequency fields couple much more strongly to tissues than do low frequency fields.¹¹ Besides, the HF-AMF instruments, usually designed for small area treatment, are always sophisticated and costly. Low frequency alternating magnetic fields (LF-AMF), 0.1-5 kHz, was recently found to be also able to promote drug permeation from magnetoliposomes with several hours' exposure time.^{12,13} Nevertheless extended exposure to power frequency (50-60 Hz) alternating fields was even revealed to increase the risk of childhood leukemia.^{14,15} Thus the exploit of ELF-MF with shortened exposure time as an effective stimulus to trigger the drug release is highly demanding.

On the other hand, to ensure the precision and accuracy of drug delivery, plenty of efforts are being carried out to visualize and monitor the local drug delivery in recent years. E.g. the delivery of doxorubicin (DOX) by unimolecular micelle was monitored by positron emission tomography (PET).^{16,17} Upconversion nanophosphor with folic acid as a tumour targeting ligand for the delivery of paclitaxel was visualized with the help of X-ray excitation.¹⁸ MRI avoiding the use of radioisotopes while providing high spatial resolution and anatomical details with real time validation, is considered as another alternative technique. Drug carriers such as liposomes, incorporated with contrast agents, were designed and investigated under MRI guidance.¹⁹ Prussian blue nanoparticles were fabricated and used as T1 contrast agent, after covalently bonded with drug molecules, the drug could be delivered under the surveillance by cellular imaging.²⁰

Herein, an ELF-MF with frequency of 20 Hz was studied to trigger the drug release. ZIF-90 was selected as the drug carrier because its small pore size resulted in relatively slow drug leakage, which enabled high percentage of drug reaching the targeting site. The particle size and surface functionalization were optimized to ensure good suspension and long blood

^a Address here. Department of Materials Science & Engineering, Faculty of Engineering, National University of Singapore, 7 Engineering Drive 1, 117574, Singapore. E-mail: msdingj@nus.edu.sg.

^b Address here. Department of Chemistry, Faculty of Science, National University of Singapore, 3 Science Drive 3, 117543, Singapore.

† Footnotes relating to the title and/or authors should appear here.

Electronic Supplementary Information (ESI) available: [Experimental details; TEM and SEM images of ZIF-90 synthesized at different conditions and discussion; TEM images of Fe₃O₄ and Gd₂O₃ nanoparticles; XRD pattern of Gd₂O₃ nanoparticles; FT-IR spectra of ZIF-90, ZIF-90-RSA and RSA; DLS of ZIF-90-RSA; UV-Vis spectra of released 5-Fu; molecular models of ZIF-90 and 5-Fu]. See DOI: 10.1039/x0xx00000x

circulation time. Superparamagnetic nanoparticles were embedded acting as actuator responsive to external ELF-MF stimulation. These embedded superparamagnetic nanoparticles would also provide effective MRI T2 contrast effect to visualize and trace the drug delivery and ensure its precision and accuracy. Alternatively, ultra-small Gd₂O₃ nanoparticles may be embedded instead of Fe₃O₄ nanoparticles to provide MRI T1 contrast effect.

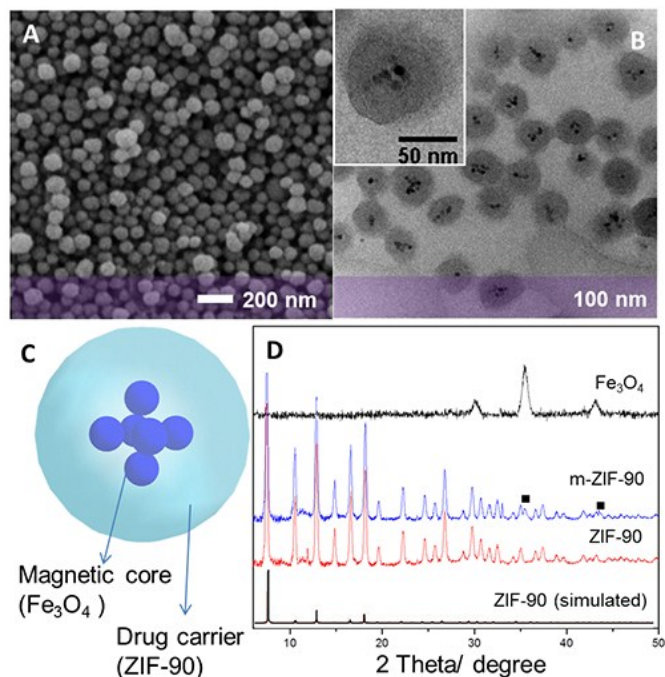


Figure 1. A, B, SEM and TEM images of m-ZIF-90. Inset B, TEM image of one m-ZIF-90 nanoparticle. C, structure illustration of m-ZIF-90. D, XRD pattern of Fe₃O₄ nanoparticles, m-ZIF-90, ZIF-90 and simulated ZIF-90, the black cubes indicate the presence of Fe₃O₄ nanoparticles in m-ZIF-90.

The preparation of homogeneous, monodispersed, and stable nanoparticles is an important issue. In some administration routes, very precise particle sizes are required, e.g. intravenous injected routes need particle size smaller than 200 nm to ensure high stable suspensions of the solids in aqueous medium and freely circulate within the smallest capillaries without aggregation. Thus particle size is a limiting factor for nanoparticles' use in biomedicine. Scaling down the size of MOFs to nanoscale regime is a vital strategy for application in DDSs.^{21,22} It is also reported by both theoretical calculations and experimental findings for various materials that the optimal particle size and surface charge for effective cellular uptake is around 50 nm with slightly negative charged surface. The further away from the optimal values, the less efficient the endocytosis of the particles is.²³⁻²⁷

Shieh *et al* reported the synthesis of ZIF-90 in water media with alcohol being co-solvent. They managed to fabricate ZIF-90 with different sizes and the smallest particle size of 275 nm.²⁸ Indeed, the co-solvent played an important role in determining the particle size. With the increase of viscosity of co-solvent, the particle size dramatically dropped. When 2-propanol was used, the average particle was above 10 μ m.

When 2-propanol was replaced by *n*-butanol, the particles immediately dropped to 3-5 μ m. The particle size further decreased to 0.5-0.8 μ m when *tert*-butanol was used instead. Recently, they further improved the synthesis procedure by using water/PVP/glycerol/*tert*-butanol system, and managed to produce 110 nm ZIF-90 nanoparticles.²⁹ In order to improve the endocytosis performance when ZIF-90 nanoparticles are used as drug carriers, the particle size has to be further reduced. Then we adopted more viscous ethylene glycol as the co-solvent, and successfully fabricated ZIF-90 nanoparticles with average size of 64 nm. (Figure 1 and Figure S1) The nanoparticles were spherical and uniform in size and morphology with narrow size distribution. This particle size is very close to the theoretical predicted and experimental proved optimal size of 50 nm. Besides, the addition of Polyvinylpyrrolidone (PVP) helped to form more uniform ZIF-90 particles. (Figure S2) And when more Zn(NO₃)₂ was used, micro-fibers were obtained rather than spherical nanoparticles (Figure S2D). Figure 1D shows the XRD pattern of the obtained cubic phased ZIF-90 nanoparticles.³⁰⁻³² The pattern agrees well with bulk ZIF-90 indicating that the pores are well maintained after scaling down to such small particle size.

Small Fe₃O₄ and Gd₂O₃ nanoparticles with size of 12 nm and 3 nm respectively were embedded in the core of ZIF-90 (m-ZIF-90 and Gd-ZIF-90 respectively). (Figure 1 and Figure S5) The presence of Fe₃O₄ nanoparticles in m-ZIF-90 can be evidenced by the XRD pattern and TEM images. (Figure 1) However, the presence of Gd₂O₃ nanoparticles in Gd-ZIF-90 was not quite obvious due to the significantly broadened XRD peaks arisen from their extremely small size as shown in Figure S3 and Figure S5. Fe₃O₄ or Gd₂O₃ nanoparticles were coated with PVP through ligand exchange with oleic acid (OA).³³ After embedded in ZIF-90, the hybrids remained their spherical morphologies and particle sizes. The TEM images confirmed the functional nanoparticles embedded in the center of ZIF-90 without any empty particles. In each m-ZIF-90 particle, an average of four Fe₃O₄ nanoparticles were embedded, while the incorporation of Gd₂O₃ nanoparticles in ZIF-90 can be much more because of their smaller size. The embedded nanoparticles can be reduced by applying less in the starting mixture. But when more functional nanoparticles were applied, the spherical morphology was destroyed and some of the functional nanoparticles appeared unwrapped under TEM observation.

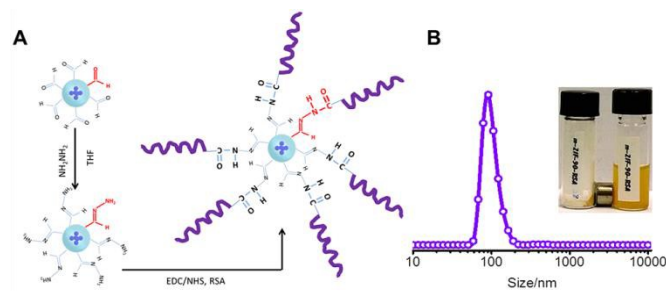


Figure 2. A, Schematic illustration of PSM of ZIF-90. B, Hydrodynamic size distribution of ZIF-90-RSA. Inset B, digital image of m-ZIF-90-RSA powder (left) attracted to an external magnet and its stable suspension in 1x PBS (right).

For bio-application, the surface modification is another important aspect since it could not only reduce the interaction with the biologic medium to improve stabilities of nanoparticles but also facilitate drug's crossing physiological barriers, thereby providing the possibility to achieve targeted delivery. Despite these virtues, the related studies in surface modification aspect are quite rare at the outset of research of MOFs in drug delivery system.²² Cochen *et al* have developed several methods to modify the amine group terminated MOFs.^{34,35} Park *et al* grafted protein onto MOFs with carboxylic acid groups on the surface.³⁶ Despite these successes made to certain MOFs, the post-synthesis modification (PSM) of most of other MOFs is still challenging due to the sensitivity of many kinds of MOFs to reaction conditions such as pH, temperature, solvent and *etc*.

The as-prepared ZIF-90 showed poor dispersion in water. But the reactive formyl group from imidazole-2-carboxyaldehyde (2-ICA) made the surface modification possible. Indeed, the PSM was successfully performed on ZIF-90 by covalent bonding with ethanolamine or reduction to hydroxyl groups in methanol at 60 °C.^{37,38} However, in our case, the direct conjugation of rat serum albumin (RSA) onto ZIF-90 was not quite successful. This may be due to the stereochemistry effect resulted from the large molecules of RSA. To reduce the steric hindrance, a small molecule hydrazine was first bonded to ZIF-90 as a linker to conjugate with RSA through peptide bond. (Figure 2A) After the bio-conjugation, the nanoparticles showed good suspension in 1xPBS solution with a narrowly distributed hydro-dynamic size around 99 nm. (Figure 2B) The zeta potential was measured to be -18 in 1x PBS solution which provides strong repulsion force among particles and enables stable suspension. (Figure 2 inset B) The strong absorption at 1033 cm⁻¹ in Fourier transform infrared spectroscopy (FT-IR) measurement contributed to the N-N stretching of ZIF-90-RSA, which indicated the successful conjugation of RSA to ZIF-90 through the hydrazone bond. (Figure S6) It was also evidenced by UV-Vis absorption at 430 nm shown in Figure S7.

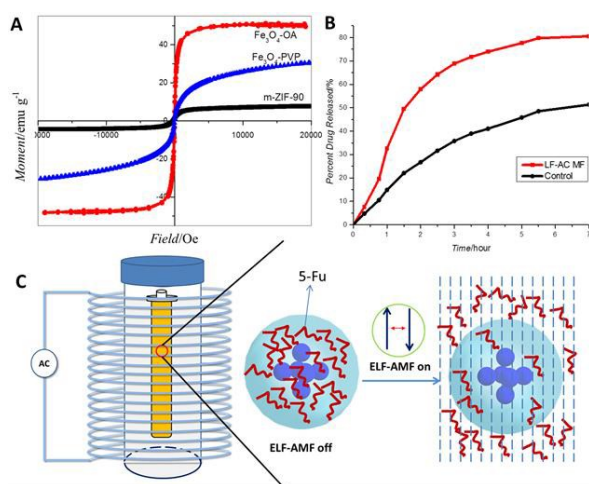


Figure 3. A, room-temperature magnetization curves of Fe₃O₄-OA, Fe₃O₄-PVP and m-ZIF-90. B, plot of 5-Fu release profile from m-ZIF-90 with and without ELF-AMF. C, Schematic illustration of 5-Fu released from m-ZIF-90 under ELF-AMF.

The magnetic property measurement of m-ZIF-90 was carried out by vibrating sample magnetometer (VSM). (Figure 3A) The OA coated Fe₃O₄ nanoparticles (Fe₃O₄-OA) showed superparamagnetism with saturated magnetism of 49 emu g⁻¹. After ligand exchange with PVP, the coating became much thicker due to the high molecular weight of PVP.³³ The saturated magnetism dropped to 32 emu g⁻¹. The value was then further reduced to 7 emu g⁻¹ after embedded in ZIF-90 which indicated the mass of Fe₃O₄ only took up about 1/7 in the composite. The powder sample can still be attracted by an external magnet as shown in Figure 2 inset B. All these three sample were superparamagnetic with the evidence of no obvious coercivity. The finding agrees with the TEM observation that the particles were discrete without agglomeration after embedded in ZIF-90.

The DDSs are expected to hold the drug after administration or injection, and immediately release it once reaching the targeting site so that the local drug concentration will achieve certain high level to be effective to kill the cancer cells. Figure S9 shows the molecular models of ZIF-90 and 5-Fu presenting a relative comparison of the drug molecule and pore size. In the current case, 5-Fu was gradually released from m-ZIF-90 without external magnetic treatment. After 1.5 hours, about 22% of 5-Fu was released, and only 50% was released after 7 hours. The small but elastic pores of m-ZIF-90 and surface functionalization by RSA may contribute to this slow drug release. When ELF-AMF with frequency of 20 Hz was applied for 20 min in every one hour in the first 7 hours as illustrated in Figure 3B, the drug release can be dramatically accelerated where more than 50% was released in the first 1.5 hours, and after 7 hours more than 80% was released, while it took around 40 hours for the controlled experiment to reach 80% drug release. (Figure S8) However, when the ELF-AMF was continuously applied for 3 successive hours, it did not show any more acceleration (data not shown) compared with ELF-AMF applied at intervals. Moreover, different extremely low frequencies (20 Hz, 40 Hz and 70 Hz) were studied to investigate their effect over the drug release performance. However, no significant difference was observed. It is indeed practically important to accelerate the release drug on command so that the local concentration immediately reaches a higher therapeutical level. Whereas in a gradual release, the spontaneous drug diffusion lowers the local drug concentration and make it insufficient to be effective.

When a magnetic material is treated under AMF, its specific absorption rate (SAR) is proportional to the frequency of AMF:

$$SAR = \frac{P}{\rho} = \pi \mu_0 \chi_0 H_0^2 f \frac{1}{\rho}$$

where SAR is expressed as W g⁻¹ of Fe, $\mu_0 = 4\pi \times 10^{-7}$ N A⁻² is the permeability of free space, H_0^2 (Am⁻¹) is the magnetic field intensity in the material, ρ is the density of the magnetic material, f is the field frequency and χ_0 is the imaginary component of complex susceptibility.^{3,39} Thus HF-AMF is always required to generate sufficient heat to stimulate the drug release. Indeed, under a commonly used 488 KHz HF-

AMF, the same concentration of m-ZIF-90 (0.1 mM Fe) treated for 10 min induced about 15 °C temperature rising due to the magnetic hyperthermia effect. While there is no detectable temperature rising even after continuously 3 hours' treatment under 20 Hz ELF-AMF.

Moreover, the embedded Fe₃O₄ or Gd₂O₃ nanoparticles can be used for MRI T₂ or T₁ contrast agents. Thus the drug delivery process can be real-timely traced and monitored by MRI. In the current case, the r₂ value of m-ZIF-90 is 133.7 and r₁ value of Gd-ZIF-90 is 4.7 at 7T. The values are comparable to commercially available MRI contrast agents. As shown in Figure 4, the T₂ or T₁ phantom images of m-ZIF-90 or Gd-ZIF-90, the darkening or brightening effect provide effective contrast to enable the visualization of the movement of the DDSs.

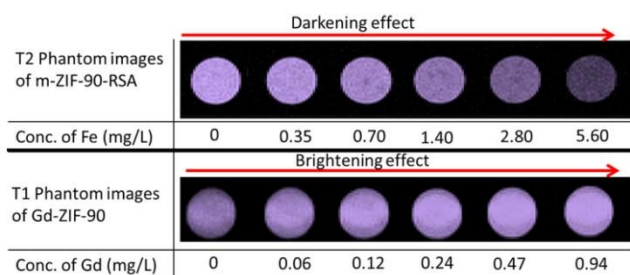


Figure 4. T₂ and T₁ phantom images of m-ZIF-90-RSA and Gd-ZIF-90-RSA with different Fe and Gd concentrations.

Conclusions

In conclusion, the particle size of ZIF-90 was successfully scaled down to 64 nm. The particle surface was PSM and conjugated with RSA to improve the water suspension and blood circulation. The resulting ZIF-90 embedded with Fe₃O₄ nanoparticles was found to be able to hold 5-Fu for quite long time. There was only 50% drug release after 7 hours. ELF-AMF with frequency of 20 Hz was found to remarkably accelerate the drug release from m-ZIF-90. 50% drug release was shortened from 7 hours without ELF-AMF treatment to only 1.5 hours with ELF-AMF treatment. Instead of being exposed to ELF-AMF continuously for several hours, ELF-AMF applied at intervals could comparably accelerate the drug release so that the exposure time could be reduced by 2/3. The acceleration of drug release on command provides a higher level of drug concentration for effective therapeutical purpose. Gd₂O₃ or Fe₃O₄ nanoparticles could be embedded as MRI T₁ or T₂ contrast tracer for potentially visualize the travel of DDSs. This DDS may be potentially used for precise drug delivery under MRI surveillance.

Notes and references

- 1 C. Alvarez-Lorenzo, A. Concheiro, *Chem. Commun.* 2014, **50**, 7743.
- 2 J.-H. Lee, J.-t. Jang, J.-s. Choi, S. H. Moon, S.-h. Noh, J.-w. Kim, J.-G. Kim, I.-S. Kim, K. I. Park, J. Cheon, *Nat. Nano.* 2011, **6**, 418.

- 3 X. L. Liu, H. M. Fan, J. B. Yi, Y. Yang, E. S. G. Choo, J. M. Xue, D. D. Fan, J. Ding, *J. Mater. Chem.* 2012, **22**, 8235.
- 4 Y. Yang, X. Liu, Y. Lv, T. S. Heng, X. Xu, W. Xia, T. Zhang, J. Fang, W. Xiao, J. Ding, *Adv. Funct. Mater.* 2015, **25**, 812.
- 5 T. T. T. N'Guyen, H. T. T. Duong, J. Basuki, V. Montembault, S. Pascual, C. Guibert, J. Fresnais, C. Boyer, M. R. Whittaker, T. P. Davis, L. Fontaine, *Angew. Chem. Inter. Ed.* 2013, **52**, 14152.
- 6 F. Lu, A. Popa, S. Zhou, J.-J. Zhu, A. C. S. Samia, *Chem. Commun.* 2013, **49**, 11436.
- 7 R. Regmi, S. R. Bhattarai, C. Sudakar, A. S. Wani, R. Cunningham, P. P. Vaishnava, R. Naik, D. Oupicky, G. Lawes, *J. Mater. Chem.* 2010, **20**, 6158.
- 8 P. M. Peiris, L. Bauer, R. Toy, E. Tran, J. Pansky, E. Doolittle, E. Schmidt, E. Hayden, A. Mayer, R. A. Keri, M. A. Griswold, E. Karathanasis, *ACS Nano*, 2012, **6**, 4157.
- 9 F. Domenico, S. Sergio, *BioMed. Eng. OnLine* 2004, **3**, 11.
- 10 International Agency for Research on Cancer, "IARC classifies radiofrequency electromagnetic fields as possibly carcinogenic to humans", Press Release No 2008, 2011.
- 11 I. Nair, M. G. Morgan, H. K. Florig, *Biological Effects of Power Frequency Electric and Magnetic Fields-Background Paper*, Washington, DC: U.S. Government Printing Office, 1989.
- 12 S. Nappini, F. B. Bombelli, M. Bonini, B. Norden, P. Baglioni, *Soft Matter* 2010, **6**, 154.
- 13 S. Nappini, M. Bonini, F. B. Bombelli, F. Pineider, C. Sangregorio, P. Baglioni, B. Norden, *Soft Matter* 2011, **7**, 1025.
- 14 M. L. McBride, R. P. Gallagher, G. Thériault, B. G. Armstrong, S. Tamaro, J. J. Spinelli, J. E. Deadman, S. Fincham, D. Robson, W. Choi. *Am. J. Epidemiol.* 1999, **149**, 831;
- 15 UK Childhood Cancer Study Investigators, *Lancet.* 1999, **354**, 1925.
- 16 Y. Xiao, H. Hong, A. Javadi, J. W. Engle, W. Xu, Y. Yang, Y. Zhang, T. E. Barnhart, W. Cai, S. Gong, *Biomater.* 2012, **33**, 3071.
- 17 R. Chakravarty, H. Hong, W. Cai, *Mol. Pharmaceutics* 2014, **11**, 3777.
- 18 H. Chen, S. He, *Mol. Pharmaceutics* 2015, **12**, 1885.
- 19 S. Langereis, T. Geelen, H. Grull, G. J. Strijkers, K. Nicolay, *NMR Biomed.* 2013, **26**, 728.
- 20 M. Shokouhimehr, E. S. Soehnlén, J. Hao, M. Griswold, C. Flask, X. Fan, J. P. Basilion, S. Basu, S. D. Huang, *J. Mater. Chem.* 2010, **20**, 5251.
- 21 P. Horcajada, R. Gref, T. Baati, P. K. Allan, G. Maurin, P. Couvreur, G. Férey, R. E. Morris, C. Serre, *Chem. Rev.* 2012, **112**, 1232.
- 22 C.-Y. Sun, C. Qin, X.-L. Wang, Z.-M. Su, *Expert Opin. Drug Deliv.* 2013, **10**, 89.
- 23 S. Zhang, J. Li, G. Lykotrafitis, G. Bao, S. Suresh, *Adv. Mater.* 2009, **21**, 419.
- 24 C. He, Y. Hu, L. Yin, C. Tang, C. Yin, *Biomater.* 2010, **31**, 3657.
- 25 S. Hirn, M. Semmler-Behnke, C. Schleh, A. Wenk, J. Lipka, M. Schäffler, S. Takenaka, W. Möller, G. Schmid, U. Simon, W. G. Kreyling, *Eur. J. Pharm. Biopharm.* 2011, **77**, 407.
- 26 S. Kulkarni, S.-S. Feng, *Pharm. Res.* 2013, **30**, 2512.
- 27 F. Lu, S.-H. Wu, Y. Hung, C.-Y. Mou, *Small* 2009, **5**, 1408.
- 28 F.-K. Shieh, S.-C. Wang, S.-Y. Leo, K. C. W. Wu, *Chem. Eur. J.* 2013, **19**, 11139.
- 29 W.-S. Lo, S.-M. Liu, S.-C. Wang, H.-P. Lin, N. Ma, H.-Y. Huang, F.-K. Shieh, *RSC Adv.* 2014, **4**, 52883.
- 30 J. A. Thompson, C. R. Blad, N. A. Brunelli, M. E. Lydon, R. P. Lively, C. W. Jones, S. Nair, *Chem. Mater.* 2012, **24**, 1930.
- 31 A. F. Gross, E. Sherman, J. J. Vajo, *Dalt. Trans.* 2012, **41**, 5458.
- 32 W. Morris, C. J. Doonan, H. Furukawa, R. Banerjee, O. M. Yaghi, *J. Am. Chem. Soc.* 2008, **130**, 12626.

- 33 J. Fang, P. Chandrasekharan, X.-L. Liu, Y. Yang, Y.-B. Lv, C.-T. Yang, J. Ding, *Biomater.* 2014, **35**, 1636.
- 34 K. K. Tanabe, Z. Wang, S. M. Cohen, *J. Am. Chem. Soc.* 2008, **130**, 8508.
- 35 Z. Wang, S. M. Cohen, *Angew. Chem. Inter. Ed.* 2008, **47**, 4699.
- 36 S. Jung, Y. Kim, S.-J. Kim, T.-H. Kwon, S. Huh, S. Park, *Chem. Commun.* 2011, **47**, 2904.
- 37 W. Morris, C. J. Doonan, H. Furukawa, R. Banerjee, O. M. Yaghi, *J. Am. Chem. Soc.* **2008**, *130*, 12626.
- 38 A. Huang, J. Caro, *Angew. Chem. Inter. Ed.* **2011**, *50*, 4979.
- 39 B. A. Bornstein, P. S. Zouranjian, J. L. Hansen, S. M. Fraser, L. A. Gelwan, B. A. Teicher, G. K. Svensson, *Int. J. Radiat. Oncol. Biol. Phys.* **1993**, *25*, 79.